ISSN 0031-918X, The Physics of Metals and Metallography, 2008, Vol. 106, No. 6, pp. 577–589. © Pleiades Publishing, Ltd., 2008.
Original Russian Text © E.Yu. Panchenko, Yu.I. Chumlyakov, I.V. Kireeva, A.V. Ovsyannikov, H. Sehitoglu, I. Karaman, Y.H.J. Maier, 2008, published in Fizika Metallov i Metallovedenie, 2008, Vol. 106, No. 6, pp. 597–609.

STRUCTURE, PHASE TRANSFORMATIONS, AND DIFFUSION

Effect of Disperse Ti_3N_4 Particles on the Martensitic Transformations in Titanium Nickelide Single Crystals

E. Yu. Panchenko[a], Yu. I. Chumlyakov[a], I. V. Kireeva[a], A. V. Ovsyannikov[a], H. Sehitoglu[b], I. Karaman[c], and Y. H. J. Maier[d]

[a] *Siberian Physicotechnical Institute, Tomsk State University, pl. Novosobornaya 1, Tomsk, 634050 Russia*
[b] *University of Illinois of Urbana, W. Green St. 1206, Urbana, IL 61801 USA*
[c] *Department of Mechanical Engineering, Texas A&M University, College Station, TX 77843 USA*
[d] *University of Paderborn, Lehrstuhl für Werkstoffkunde (Material Science), Pohlweg 47-49, Paderborn, 33098 Germany*

Received January 28, 2008

Abstract—The effect of the size and volume fraction of Ti_3N_4 particles in Ti–(50.3–51.5) at % Ni single crystals on their martensitic transformation temperatures and temperature hysteresis is studied. Aging at T = 673–823 K leads to a nonmonotonic change in the martensitic transformation temperatures and temperature hysteresis, which is related to a change in the Ni concentration in the matrix, the hardening of the high-temperature phase, a change in the elastic and surface energies generated upon the martensitic transformations, and the internal stresses that appear because of the difference in the lattice parameters of the particles and the matrix. As a result of the high strength of the $B2$ phase and the high elastic and surface energies that are generated upon the martensitic transformations due to the precipitation of particles of size $d < 40$ nm at an interparticle distance $\lambda < 50$ nm, the martensitic transformation temperatures decrease down to the suppression of the R–$B19'$ transitions upon cooling to 77 K. A thermodynamic description for the martensitic transformations in heterophase crystals is proposed, and an analogy between the martensitic transformations in heterophase Ti–Ni single crystals with nanoparticles of size d = 20–100 nm and those in single-phase Ti–Ni polycrystals with a grain size of 50–200 nm is found.

PACS numbers: 81.30.Kf, 81.40.-z

DOI: 10.1134/S0031918X08120065

INTRODUCTION

The temperatures of the start (M_s) and finish (M_f) of the martensitic transformation (MT) and the temperatures of the start (A_s) and finish (A_f) of the reverse martensitic transformation in Ti–Ni alloys are known to depend on the Ni concentration, the dislocation density, the number of disperse particles, and the grain size [1–3]. A high dislocation density, the precipitation of fine (d < 20 nm) Ti_3Ni_4 particles, and a decrease in the grain size to d = 50–200 nm decrease the M_s temperature and can even suppress the martensite transformation into the $B19'$ monoclinic martensite by stabilizing the $B2$ phase [1–5]. The MTs in heterophase Ti–Ni alloys with disperse Ti_3Ni_4 particles have a number of specific features as compared to the related single-phase alloys:

(i) The single-phase alloys undergo a one-stage $B2$–$B19'$ MT, and the precipitation of the particles leads to a two-stage ($B2$–R–$B19'$) transformation through the intermediate rhombohedral R phase [1–4].

(ii) The disperse particles change the type of twinning in $B19'$ martensite crystals from the second-type $\langle 011\rangle\{0.72053\ 1\ 1\}$ twinning to the compound $\langle 001\rangle\{100\}$ twinning, and the density of compound twins increases as the interparticle distance λ decreases [6].

(iii) The disperse Ti_3Ni_4 particles have a rhombohedral structure, which differs from that of the $B2$ matrix, and do not undergo the MT. Because of the difference in the lattice parameters of the $B2$ matrix and the Ti_3Ni_4 particles, they serve as sources of internal stresses and favor the nucleation of R and $B19'$ martensite crystals at the particle–matrix interface [1–4, 6–10].

Upon aging of Ti–Ni polycrystals with a nickel concentration $C_{Ni} \geq 50.6$ at %, Ti_3Ni_4 particles precipitate predominantly along grain boundaries, which results in a nonuniform particle distribution in the bulk of grains and the near-boundary regions [3, 8, 9]. As a result, multistage Ç2–R and Ç2–$B19'$ MTs occur; these are related to the chemical heterogeneity and internal stresses induced by disperse particles [8–13]. Using Ti–Ni single crystals to study thermoelastic MTs, we can avoid the difficulties related to the heterogeneous nucleation of particles in polycrystals. The purpose of this work is to investigate the effect of Ti_3Ni_4 particles on the development of the thermoelastic MTs in Ti–Ni single crystals during cooling/heating.

EXPERIMENTAL

We studied Ti–50.3 at % Ni, Ti–50.5 at % Ni, Ti–50.7 at % Ni, Ti–50.8 at % Ni, Ti–51.0 at % Ni, and Ti–51.5 at % Ni alloy single crystals grown by the Bridgman technique in an inert gas atmosphere. After growing, the single crystals were homogenized at 1173 K for 20 h in argon. To form a single-phase state, we held samples at 1203 K for 0.5 h and quenched them in water at room temperature. Tensile specimens with a $3.0 \times 1.5 \times 16.0$-mm gage portion were spark cut. The MT temperatures were determined from the temperature dependence of the electrical resistivity and by differential scanning calorimetry (DSC) at a heating/cooling rate of 10 K/min in the temperature range 120–370 K. Before tests, the specimens were ground and electrolytically polished in a 5% $HClO_4$ + 95% CH_3COOH electrolyte at $T = 293$ K and $U = 22$ V.

Ni-rich ($C_{Ni} \geq 50.7$ at % Ni) Ti–Ni single crystals were aged at $T = 573$–823 K for 1.0–1.5 h in a free-standing state in a helium atmosphere with rapid heating followed by water quenching at room temperature.

The microstructures of the aged Ti–Ni alloy samples were studied in an EM-125 transmission electron microscope at an accelerating voltage of 125 kV. The foils for examination were prepared by jet polishing in a 20% H_2SO_4 + 80% CH_3OH electrolyte. The size (d) and volume fraction (f) of particles and the average interparticle distance λ were determined by the procedure described in [11]. The nickel concentration C_{Ni} in an aged matrix was estimated by the formula [14]

$$C'_{Ni} = \frac{C_{Ni} - Af}{1 - f}, \quad (1)$$

where C_{Ni} is the Ni concentration in the quenched crystal (at %), C'_{Ni} is the Ni concentration in the single-crystal matrix after aging (at %), $A \approx 56.0$ at % is the Ni concentration in a Ti_3Ni_4 ($Ti_{11}Ni_{14}$) particle [7], and f is the volume fraction of particles. When determining the error of calculating the residual Ni concentration in an aged matrix C'_{Ni}, we only took into account the error in calculating the volume fraction of disperse particles f. The mechanical tests of the specimens were performed by tension to find the strength properties of the high-temperature $B2$ phase in the single-phase state and after aging, and the strain rate was $\dot{\varepsilon} = 4 \times 10^{-4}$ 1/s.

RESULTS AND DISCUSSION

Figure 1 shows the effect of the Ni concentration on the $B2$–$B19'$ MT temperatures for single-phase Ti–Ni single crystals. The M_s and M_f temperatures of the $B2$–$B19'$ transformation and the A_s and A_f temperatures of the $B19'$–$B2$ transformation were determined from inflection points in the temperature dependence of electrical resistivity $\rho(T)$ upon cooling and heating. The M_s temperature is seen to decrease with increasing nickel concentration and becomes lower than 77 K at $C_{Ni} \geq 51.5$ at %. As follows from Fig. 1, the temperature ranges of the forward ($\Delta_1 = M_s - M_f$) and reverse ($\Delta_2 = A_f - A_s$) MTs and the thermal hystereses $\Gamma_1 = A_f - M_s$ and $\Gamma_2 = A_s - M_f$ are equal to each other, i.e., $\Delta_1 = \Delta_2$ and $\Gamma_1 = \Gamma_2$.

Aging of Ti–Ni crystals with $C_{Ni} \geq 50.7$ at % leads to the precipitation of disperse Ti_3Ni_4 particles. As is seen from Fig. 2 and Table 1, the particle size d, the interparticle distance λ, and the volume fraction of Ti_3Ni_4 particles f depend on the Ni concentration and the aging temperature and time. Upon aging in a free-standing state, four crystallographically equivalent versions of particles precipitate. In the rhombohedral axes, they have the following orientation relationships with the $B2$ matrix [2]:

$$(111)_{Ti_3Ni_4} \parallel (111)_{B2} \quad [101]_{Ti_3Ni_4} \parallel [321]_{B2}.$$

When Ti–Ni crystals with disperse Ti_3Ni_4 particles are cooled, the martensite transformation from the $B2$ phase into the rhombohedral R phase first takes place at $T = T_R$, which is detected from an increase in the electrical resistivity in the $\rho(T)$ curves. This increase in $\rho(T)$ corresponds to a heat-release peak in the DSC curves (Fig. 3). A further decrease in the temperature results in the R–$B19'$ MT, which corresponds to a decrease in $\rho(T)$ and to the second heat-release peak. The reverse MT has one stage ($B2$–$B19'$), and one heat-absorption peak is observed upon heating. Figure 4 shows the $\rho(T)$ dependence for aging of nickel-rich Ti–Ni crystals ($C_{Ni} = 50.7$ at %) under various conditions. Figure 5 shows the dependences of the MT temperatures on the size and volume fraction of particles. As follows from these results, the temperature T_R of the onset of the $B2$–R transformation weakly depends on the alloy composition and the aging time and temperature, whereas the M_s and M_f temperatures of the R–$B19'$ transformation and the A_s and A_f temperatures of the $B19'$–$B2$ transformation substantially depend on the size and volume fraction of disperse Ti_3Ni_4 particles (Fig. 5). In the Ti–50.7 at % Ni ($f = 4\%$) and Ti–50.8 at % Ni ($f = 5\%$), M_s increases as the particle size grows from 25 to 400 nm (Figs. 5a, 5b). An increase in the volume fraction to $f = 9\%$ in the Ti–51.0 at % Ni crystals leads to a nonmonotonic dependence of M_s of the particle size. At small particle sizes ($d = 25 \pm 5$ nm) and small interparticle distances ($\lambda < 40$ nm), the R–$B19'$ transformation is suppressed upon cooling, and the M_s temperature becomes lower than 77 K (Fig. 5c). At $d > 40$ nm and $\lambda > 40$ nm, M_s increases with the particle size. The forward MT temperature range $\Delta_1 = M_s - M_f$ is found to depend on the size and volume fraction of particles. When nanoparticles ($d \leq 100$ nm) precipitate, M_f decreases substantially, and Δ_1 increases twofold or more as compared to the single-phase crystals (see Fig. 5). As the particle size grows ($d \geq 100$ nm) at $f = 4$–5% Δ_1 decreases to values close to those of the single-

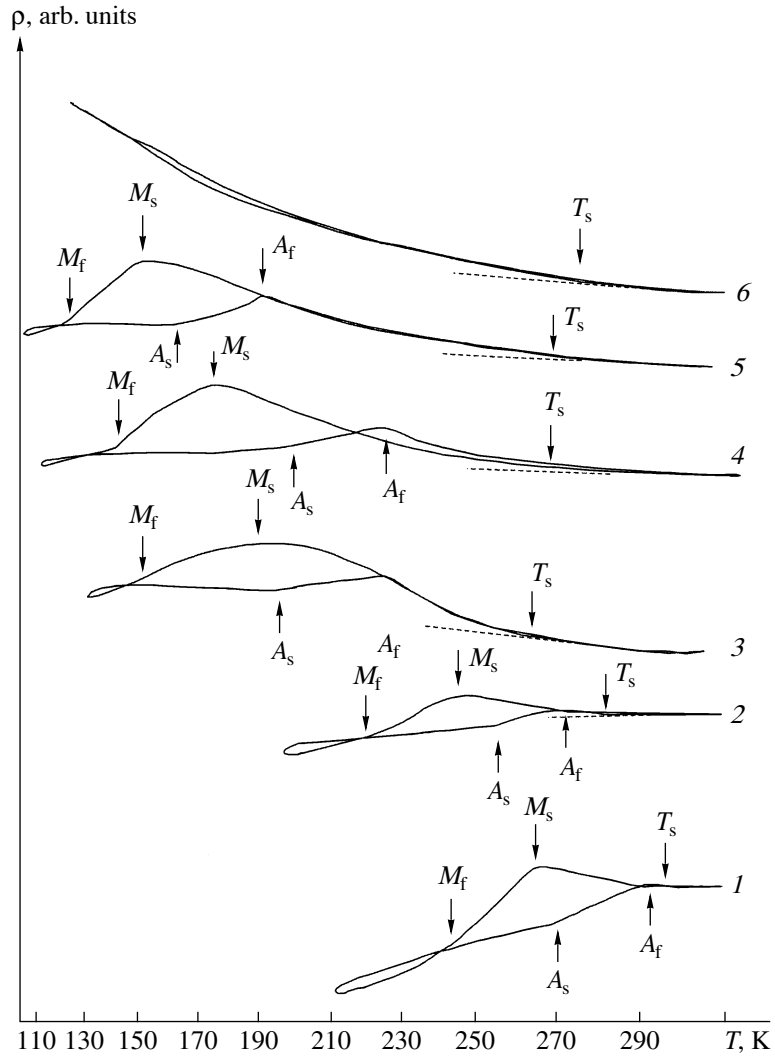

Fig. 1. Temperature dependences of the electrical resistivity of quenched Ti–Ni single crystals of various chemical compositions: (*1*) Ti–50.3 at % Ni, (*2*) Ti–50.5 at % Ni, (*3*) Ti–50.7 at % Ni, (*4*) Ti–50.8 at % Ni, (*5*) Ti–51.0 at % Ni, and (*6*) Ti–51.5 at % Ni. Temperatures M_s, M_f, A_s, and A_f are the temperatures of the start and finish of the forward and reverse *B*2–*B*19' MT upon cooling/heating, respectively. T_s is the temperature of the start of the formation of an incommensurate intermediate displacive structure (IDSs) related to the premartensitic states in Ti–Ni alloys [2].

phase crystals. In crystals with a high volume fraction of particles ($d \geq 100$ nm, $f = 9\%$), the values of Δ_1 turn out to be twice as large as those in the single-phase state and remain almost the same as the particle size grows from 100 to 400 nm (Fig. 5c). As compared to the single-phase crystals, the A_s and A_f temperatures of the reverse *B*19'–*B*2 transformation at $f = 4$–5% and $d = 25$–40 nm increase, and the temperature range of the reverse MT Δ_2 decreases significantly (Figs. 5a, 5b). Thus, in crystals with disperse particles of size $d \leq$ 40 nm, the temperature range of the forward MT Δ_1 is larger than the temperature range of the reverse MT Δ_2 by a factor of three to five, and the temperature hystereses $\Gamma_1 = A_f - M_f$ and $\Gamma_2 = A_s - M_f$ increase as compared to the single-phase crystals (see Fig. 5). The hysteresis $\Gamma_2 = A_s - M_f$ in these states turns out to be larger than Γ_1. When large (d = 100–400 nm) particles precipitate and $f = 4$–5% Γ_1, Γ_2, Δ_1, and Δ_2 decrease as compared to the crystals with small particles ($d \leq 40$ nm). It is interesting that the values of Γ_1 and Δ_1 in crystals with large ($d \geq 100$ nm) particles are close to those of single-phase crystals, whereas Δ_2 turns out to be significantly smaller than that of single-phase crystals. As a result, the following relations are characteristic of the crystals containing large and small disperse particles: $\Delta_1 > \Delta_2$ and $\Gamma_1 < \Gamma_2$. However, for small (d = 25–40 nm) particles, Δ_1 and Γ_2 significantly exceed Δ_2 and Γ_1 (Δ_1/Δ_2 = 4–5, Γ_2/Γ_1 = 2–3). For large (d = 100–400 nm) particles, these ratios decrease (Δ_1/Δ_2 = 1.6–3.8, Γ_2/Γ_1 = 1.2–1.7).

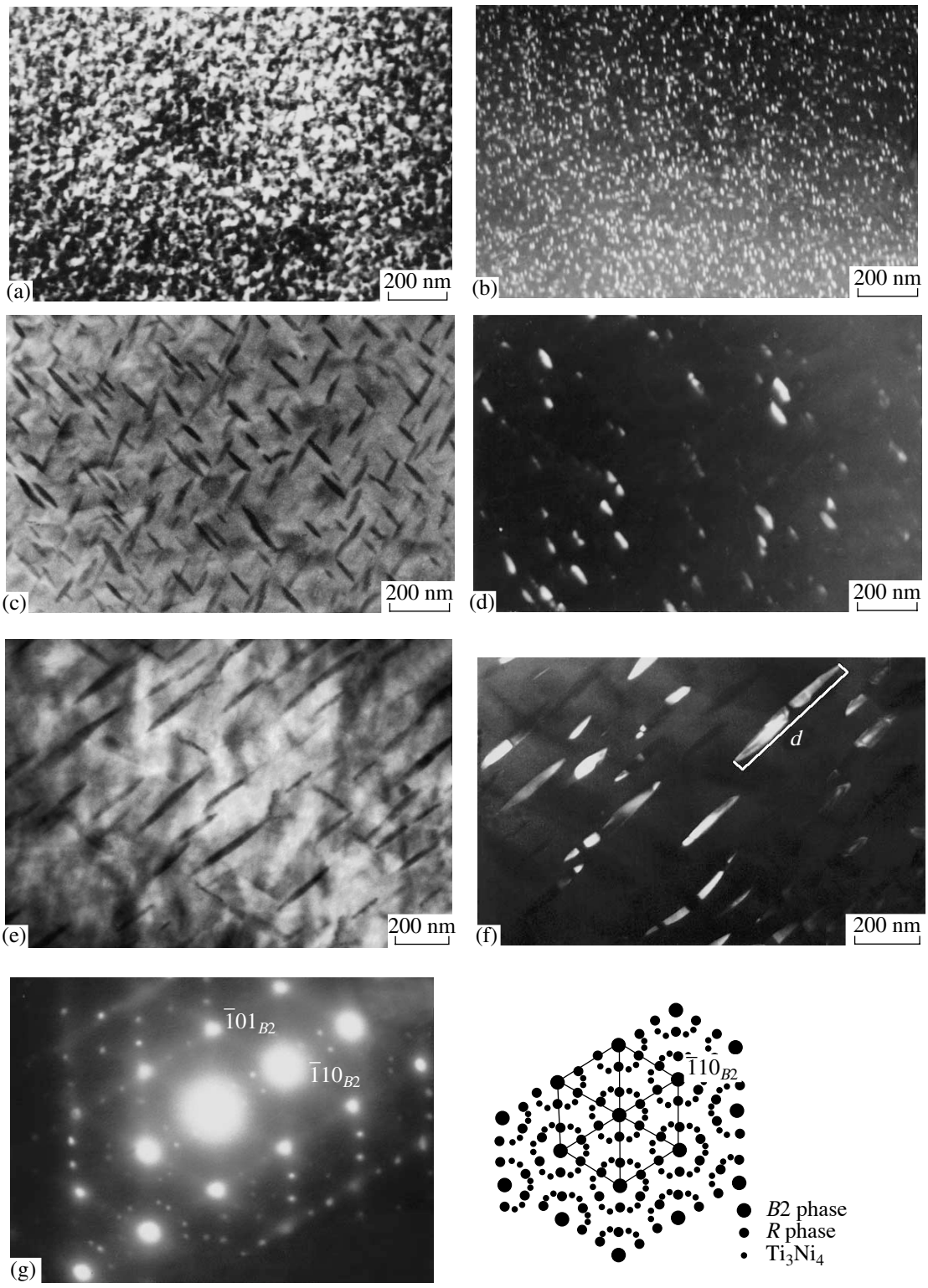

Fig. 2. Microstructure of aged Ti–51 at % Ni single crystals: (a, c, e) bright-field images, (b, d, f) dark-field images taken with a particle reflection, (a, b) after aging at 673 K for 1 h, (c, d) after aging at 773 K for 1 h, (e, f) after aging at 823 K for 1.5 h, and (g) electron diffraction pattern ~$(111)^*_{B2}$ for (e) and (f) and its key pattern. The orientation relationship $(\bar{1}10)_{B2} \parallel (300)_R \parallel (3\bar{2}\bar{1})_{Ti_3Ni_4}$ holds true.

Table 1. Microstructure parameters of aged Ti–(50.7–51.5) at % Ni single crystals

Chemical composition	Aging conditions	Particle size d, nm	Interparticle distance λ, nm	Volume fraction of particles f, %, ±0.5%	Ni concentration in the matrix after aging, $C_{Ni'}$, at %
Ti–50.7 at % Ni	673 K, 1.5 h	35 ± 5	100 ± 10	3.6	50.50
	773 K, 1 h	100 ± 10	220 ± 20	3.8	50.49
	823 K, 1.5 h	400 ± 20	550 ± 20	4.0	50.48
Ti–50.8 at % Ni	823 K, 1.5 h	360 ± 20	510 ± 20	5.0	50.53
Ti–51.0 at % Ni	673 K, 1 h	25 ± 5	35 ± 5	9.4	50.48
	673 K, 1.5 h	35 ± 5	45 ± 5	9.3	50.49
	773 K, 1 h	100 ± 10	100 ± 10	9.1	50.50
	823 K, 1.5 h	400 ± 20	370 ± 20	9.0	50.51
Ti–51.5 at % Ni	823 K, 1.5 h	400 ± 20	250 ± 10	16.0	50.64

It is known [1–3, 15, 16] that, in the absence of applied stresses, the onset of a thermoelastic MT requires a chemical driving force ΔG_{ch} to overcome an energy barrier, which is related to the generation of an elastic energy (ΔG_{el}) and a surface energy (ΔG_s) and to the work required to overcome the friction forces during the motion of the interface and dislocation formation (ΔG_{fr}). According to [15, 16], the conditions for the onset of the forward (Eq. (2)) and reverse (Eq. (3)) MTs can be written as

$$-\Delta G_{ch}^{A–M} + \Delta G_{rev}^{A–M} + \Delta G_{fr}^{A–M} = 0, \quad (2)$$

$$-\Delta G_{ch}^{M–A} - \Delta G_{rev}^{M–A} + \Delta G_{fr}^{M–A} = 0. \quad (3)$$

Here, $\Delta G_{rev} = \Delta G_{el} + \Delta G_s$ is the reversible component of the nonchemical free energy, which characterizes the

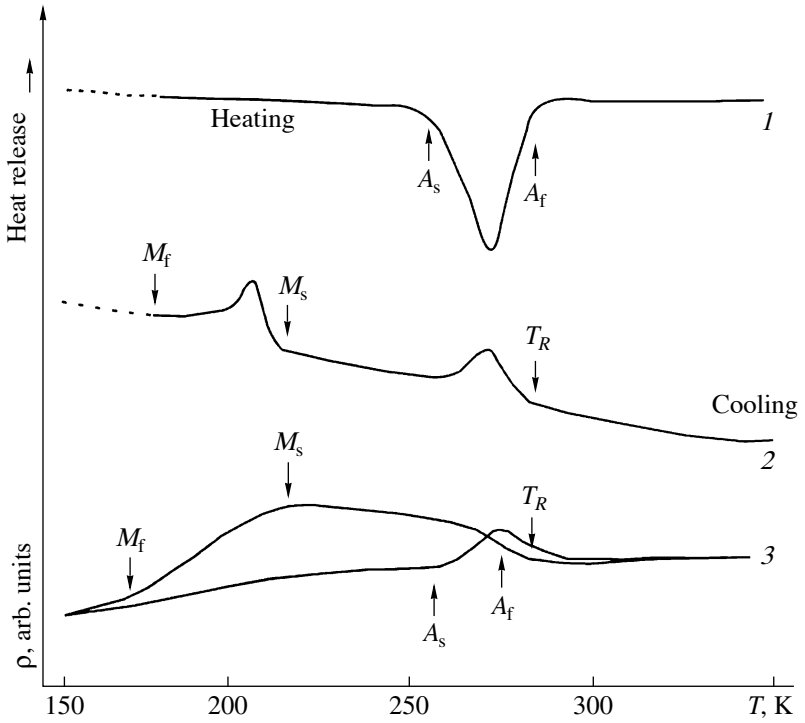

Fig. 3. (*1, 2*) DSC curves and (*3*) ρ(*T*) dependence upon cooling/heating of Ti–51 at % Ni single crystals aged at 823 K for 1.5 h. T_R is the temperature of the start of the *B*2–*R* MT upon cooling. M_s and M_f are the temperatures of the start and finish of the forward *R*–*B*19' MT upon cooling, respectively. A_s and A_f are the temperatures of the start and finish of the reverse *B*2–*B*19' MT upon heating, respectively.

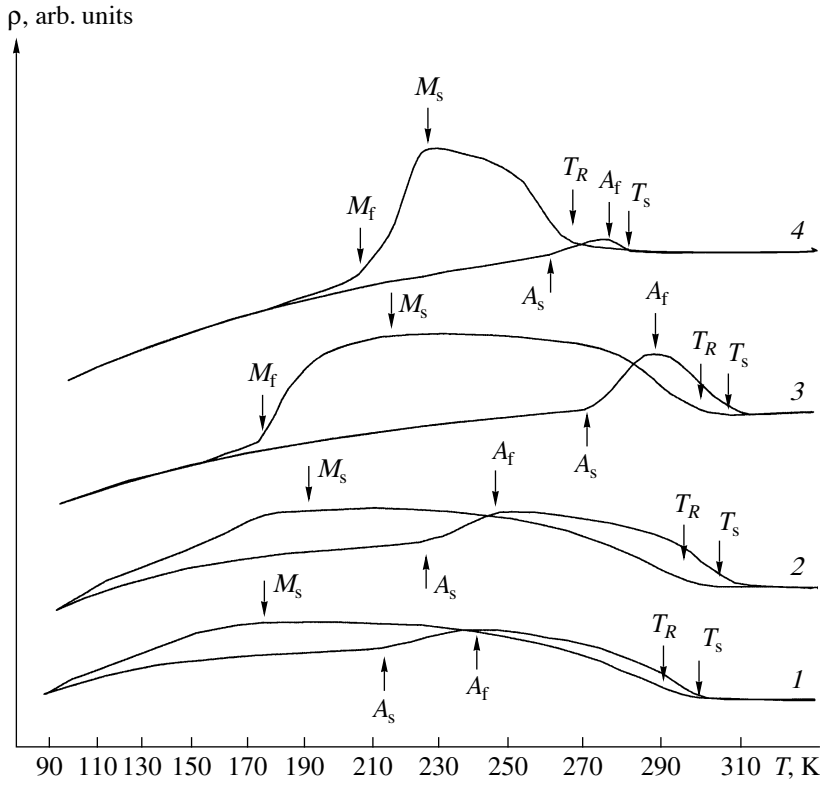

Fig. 4. Temperature dependences of the electrical resistivity of Ti–50.8 at % Ni single crystals after the following heat treatments: (*1*) quenching from 1203 K + aging at 673 K for 1 h, (*2*) quenching from 1203 K + aging at 673 K for 1.5 h, (*3*) quenching from 1203 K + aging at 773 K for 1 h, and (*4*) quenching from 1203 K + aging at 823 K for 1.5 h. T_s is the temperature of the start of the formation of IDSs related to the premartensitic states in Ti–Ni alloys [2]. T_R is the temperature of the start of the *B*2–*R* MT upon cooling. M_s and M_f are the temperatures of the start and finish of the forward *R*–*B*19' MT upon cooling, respectively. A_s and A_f are the temperatures of the start and finish of the reverse *B*2–*B*19' MT upon heating, respectively.

elastic and surface energies accumulated in the material; ΔG_{rev} depends on the volume fraction of martensite δ; ΔG_{fr} is the irreversible component of the nonchemical free energy, which characterizes the energy dissipation during an MT that is associated with the friction stresses required for the motion of the interface and with the plastic relaxation of the elastic energy due to dislocation generation; and ΔG_{fr} is assumed to be independent of the volume fraction of martensite and to remain the same for the forward and reverse MT, $\left|\Delta G_{fr}^{M–A}\right| = \left|\Delta G_{fr}^{A–M}\right| = |\Delta G_{fr}|$. We take into account that chemical phase equilibrium temperature T_0 is determined from the relation

$$\Delta G_{ch}^{A–M} = \Delta H_{ch}^{A–M} - T_0 \Delta S_{ch}^{A–M} \quad (4)$$

and use Eqs. (2) and (3) to find the MT characteristic temperatures [16]

$$M_s = T_0 - \frac{\Delta G_{rev}(0)}{\Delta S_{ch}} - \frac{\Delta G_{fr}}{\Delta S_{ch}};$$

$$M_f = T_0 - \frac{\Delta G_{rev}(1)}{\Delta S_{ch}} - \frac{\Delta G_{fr}}{\Delta S_{ch}};$$

$$A_s = T_0 - \frac{\Delta G_{rev}(1)}{\Delta S_{ch}} + \frac{\Delta G_{fr}}{\Delta S_{ch}}; \quad (5)$$

$$A_f = T_0 - \frac{\Delta G_{rev}(0)}{\Delta S_{ch}} + \frac{\Delta G_{fr}}{\Delta S_{ch}}.$$

Here, $\Delta G_{rev}(0)$ and $\Delta G_{rev}(1)$ are the elastic and surface energies accumulated in the material at a volume fraction of martensite of $\delta \longrightarrow 0$ and $\delta \longrightarrow 1$, respectively. For the forward MT, the transformation entropy is $\Delta S_{ch}^{A–M} < 0$, and, for the reverse MT, it is $\Delta S_{ch}^{M–A} > 0$. In Eq. (4), $\Delta S_{ch} = \left|\Delta S_{ch}^{A–M}\right| = \Delta S_{ch}^{M–A} = 1.953$ J/(mol K) [10].

Using the experimental MT temperatures, T_0, and Eq. (5), we can estimate the contributions of ΔG_{rev} and ΔG_{fr} to the nonchemical component of the free energy,

$$\left|\Delta G_{rev}(0)\right| = T_0 \Delta S_{ch} - (M_s + A_f)\frac{\Delta S_{ch}}{2};$$

$$|\Delta G_{rev}(1)| = T_0\Delta S_{ch} - (A_s + M_f)\frac{\Delta S_{ch}}{2}; \quad (6)$$

$$|\Delta G_{fr}| = \frac{\Delta S_{ch}}{2}(A_f - M_s).$$

To estimate $|\Delta G_{rev}|$ and $|\Delta G_{fr}|$ in single-phase Ti–Ni crystals, we used the approximation from [1, 15]. Elastic and surface energies $|\Delta G_{rev}|$ are assumed not to appear when the first martensite plate nucleates at $T = M_s$ (the volume fraction of martensite is $\delta \longrightarrow 0$); correspondingly, for the last martensite plate in the reverse MT at $T = A_f$, we have $|\Delta G_{rev}(0)| \longrightarrow 0$. In this case, the reversible energy does not affect the positions of the M_s and A_f points with respect to the chemical phase quasi-brittle fracture temperature, and T_0 is determined by the Tong–Wayman formula [1, 3, 15]

$$T_0 = \frac{M_s + A_f}{2}. \quad (7)$$

This is possible when martensite plates nucleate on free single-crystal surfaces [15, 16]. As the volume fraction of martensite increases, the reversible energy $|\Delta G_{rev}(\delta)|$ increases and achieves a maximum at $\delta \longrightarrow 1$. The calculations demonstrate that, in single-phase Ti–Ni crystals at all Ni concentrations, the reversible energy $|\Delta G_{rev}(1)|$ accumulated during the *B*2–*B*19' transformation is higher than the energy scattering $|\Delta G_{fr}|$, i.e., $|\Delta G_{rev}(1)|/|\Delta G_{fr}| = 1.2–1.5$. As a result, the temperature of the onset of the reverse MT A_f is close to T_0; hence, the reversible energy accumulated during the forward *B*2–*B*19' transformation causes the onset of the reverse MT at a near-zero chemical driving force.

As the Ni concentration in single-phase crystals increases, the nonchemical component of the free energy $|\Delta G_{rev}| + |\Delta G_{fr}|$ increases weakly: at $C_{Ni} = 50.3$ at %, $|\Delta G_{rev}(1)| = 45$ J/mol and $|\Delta G_{fr}| = 27$ J/mol; at $C_{Ni} = 51.0$ at %, $|\Delta G_{rev}(1)| = 53$ J/mol and $|\Delta G_{fr}| = 42$ J/mol. However, as is seen in Fig. 6, T_0 and M_s decrease identically with increasing Ni concentration within the limits of experimental error, and the relation $\frac{\Delta M_s}{\Delta C_{Ni}} \approx \frac{\delta T_0}{\delta C_{Ni}} \approx$ –(175 ± 10) K/at % is valid. This dependence of M_s and T_0 on the Ni concentration in Ti–Ni single crystals turns out to be close to the data obtained on coarse-grained Ti–Ni polycrystals [17].

The change in the temperature of the onset of the MT ΔM_s in Ti–Ni single crystals induced by the precipitation of disperse Ti_3Ni_4 particles as compared to the single-phase crystals can be written as [4, 18, 19]

$$\Delta M_s = \frac{\delta T_0}{\delta C_{Ni}}\Delta C_{Ni} - \frac{\delta\Delta T}{\delta\Delta\sigma_{0.1}}\Delta\sigma_{0.1} - \frac{\delta\Delta T}{\delta\Delta\sigma_i}\Delta\sigma_i + \frac{\Delta S}{\varepsilon_0}\Delta\sigma_{in}. \quad (8)$$

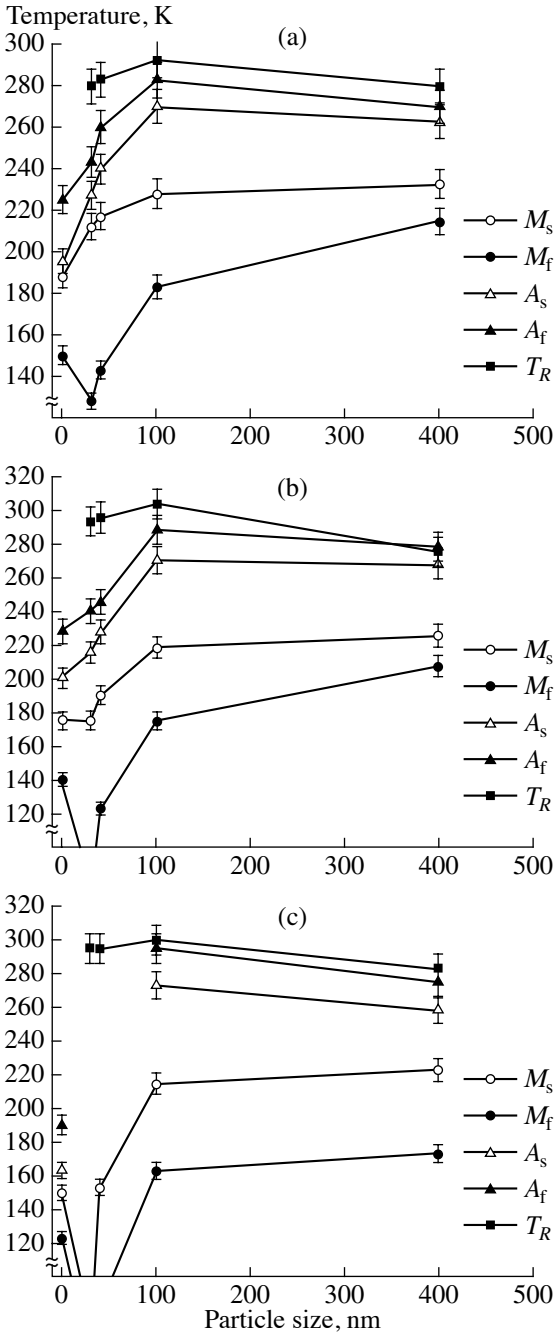

Fig. 5. *R*–*B*19' MT temperatures in quenched and aged Ti–(50.7–51.0) at % Ni single crystals containing disperse Ti_3Ni_4 particles of various sizes: (a) Ti–50.7 at % Ni ($f_{Ti_3Ni_4} = 4\%$), (b) Ti–50.8 at % Ni ($f_{Ti_3Ni_4} = 5\%$), and (c) Ti–51.0 at % Ni ($f_{Ti_3Ni_4} = 9\%$).

According to Eq. (8), ΔM_s is specified by the following factors:

(i) A change in the chemical composition of the matrix upon aging, which is described by the first term in Eq. (8) ($\frac{\delta T_0}{\delta C_{Ni}}\Delta C_{Ni}$). The decrease in the Ni content

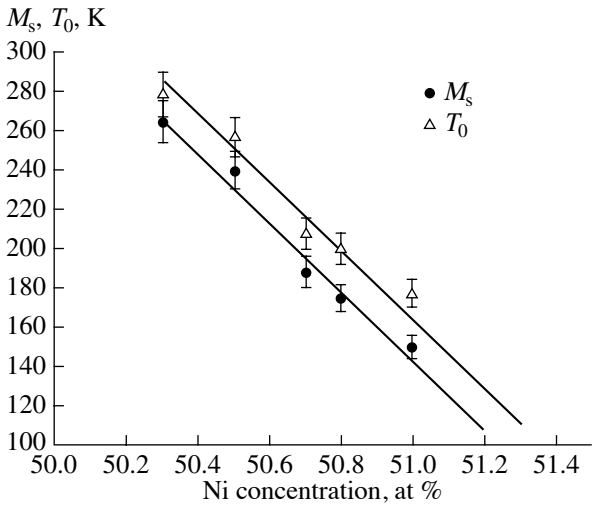

Fig. 6. Dependences of the temperature of the start of the *B*2–*B*19' MT M_s and the phase equilibrium temperature T_0 on the nickel concentration in quenched Ti–(50.3–51.0) at % Ni single crystals.

upon the precipitation of Ni-rich Ti_3Ni_4 particles leads to a Ni depletion of the matrix and to an increase in the MT temperatures ($\frac{\delta T_0}{\delta C_{Ni}}\Delta C_{Ni} > 0$).

(ii) The disperse particles increase the strength properties of the *B*2 phase, $\Delta\sigma_{0.1} = \sigma_{0.1}^{aged}(B2) - \sigma_{0.1}^{sp}(B2)$ (Table 2) [19, 20], which increases the resistance to the motion of interphase boundaries during an MT and, hence, the supercooling $\Delta T = T_0 - M_s$. Thus, the second term in Eq. (8), $\frac{\delta\Delta T}{\delta\Delta\sigma_{0.1}}\Delta\sigma_{0.1}$ decreases the M_s temperature.

(iii) When disperse Ti_3Ni_4 particles (which do not undergo an MT) precipitate in Ti–Ni crystals, the elastic energy increases additionally, as compared to the single-phase state, due to the elastic deformation of the particles during an MT [21] and to the surface energy required for the generation of a high density of compound {001}⟨100⟩ twins, which are experimentally observed in Ti–Ni crystals with particles [6]. As a result, the supercooling ΔT increases additionally and, correspondingly, M_s decreases in heterophase Ti–Ni crystals as compared to single-phase Ti–Ni crystals. This difference is described by the third term in Eq. (8), $\frac{\delta\Delta T}{\delta\Delta\sigma_i}\Delta\sigma_i$.

(iv) In heterophase crystals, the local internal stresses $\Delta\sigma_{in}$ induced by disperse particles because of the difference between the particle and matrix lattice parameters favor the nucleation of martensite crystals at particle–matrix interfaces and, according to the Clausius–Clapeyron equation [1–3], should increase the M_s temperature, $\Delta M_s = \frac{\Delta S_{ch}}{\varepsilon_0}\Delta\sigma_{in}$ (the fourth term in Eq. (8)).

The nickel concentration estimated in a matrix upon aging demonstrates that the matrix of all aged Ti–Ni single crystals with $C_{Ni} \geq 50.7$ at % has the same composition, namely, $C_{Ni} = 50.51 \pm 0.05$ at % (see Table 1). Therefore, chemical phase equilibrium temperature T_0 for all heterophase single crystals studied in this work is the same, $T_0 = 260 \pm 5$ K. Hence, in aged Ti–Ni single crystals, the dependence of M_s on the size (d) and volume fraction (f) of Ti_3Ni_4 particles and the average interparticle distance λ is determined by the dependence of the supercooling ΔT on the microstructure of the material (terms 2–4 in Eq. (8)). When large ($d >$ 100 nm) particles precipitate in heterophase crystals, M_s increases substantially (ΔM_s = 40–50 K) as compared to the corresponding single-phase crystals and weakly depends on the volume fraction of the particles. When particles of size $d \leq$ 25–30 nm precipitate, this temperature is controlled by the volume fraction of particles: at f = 9%, M_s decreases and becomes close to 77 K ($\Delta M_s \geq -70$ K) (see Fig. 5). This resistance to the

Table 2. Dependences of the yield strength of the *B*2 phase $\sigma_{0.1}(B2)$ at $T = M_d + 50$ K and the martensitic shear stress $\sigma_{0.1}(M_s)$ on the aging temperature and time in [$\bar{1}$11] Ti–51 at % Ni single crystals and these parameters for [$\bar{1}$11] single-phase Ti–50.5 at % Ni single crystals

Chemical composition of the single crystals	Heat-treatment conditions	Particle size d, nm	$\sigma_{0.1}(B2)$, MPa	$\sigma_{0.1}(M_s)$, MPa
Ti–50.5 at % Ni	Quenching from 1273 K, 0.5 h	–	520	40
Ti–51.0 at % Ni	Quenching from 1273 K, 0.5 h	–	740	170
Ti–51.0 at % Ni	Aging at 673 K, 1 h	25 ± 5	1050	160
	Aging at 673 K, 1.5 h	35 ± 5	930	140
	Aging at 773 K, 1 h	100 ± 10	800	120
	Aging at 823 K, 1.5 h	400 ± 20	620	60

Note: M_d is the temperature at which the martensitic shear stresses are equal to the yield strength of the *B*2 phase.

*R–B*19' transformation in crystals with nanoparticles of size $d \le 25$–40 nm can be explained with Eq. (8) as follows. A comparison of the development of the MTs in single-phase Ti–Ni polycrystals with a grain size D = 50–200 nm and in Ti–Ni single crystals containing disperse Ti_3Ni_4 particles with d = 20–40 nm and an interparticle distance $\lambda \le 40$ nm indicates a number of common features. First, at $D < 100$ nm, one version of martensite is detected in one grain, and a similar microstructure takes place in Ti–Ni with Ti_3Ni_4 particles at $\lambda \le 100$ nm [5]. Second, at $D \le 200$ nm in single-phase Ti–Ni alloys and at $\lambda \le 100$ nm in Ti–Ni with disperse particles, the martensite contains compound twins, and their density increases with decreasing λ and D [6, 22]. Compound $\{001\}\langle 100\rangle$ twins should be considered as "geometrically necessary defects" that appear to match the elastic deformation of the particles with the martensitic deformation of the matrix. The density of such defects ρ_G can be estimated using the gradient theory of plasticity [23], which was developed for the plastic deformation of composites in which one component (particle) can only elastically be deformed and the matrix is plastically deformed:

$$\rho_G = \frac{1}{b}\frac{\gamma}{\lambda}. \quad (9)$$

Here, b is the Burgers vector of the compound $\langle 100\rangle\{001\}$ b twins (b = 0.231 nm), γ is the martensitic shear upon the *R–B*19' transformation (0.130 [3]), and λ is the distance between particles (see Table 1) or other obstacles hindering this MT (e.g., grain boundaries in Ti–Ni polycrystals). Our estimations demonstrate that, in the single crystals under study, the compound-twin density is maximal in crystals with small disperse particles ($d = 25 \pm 5$ nm): at f = 9%, it is $\rho_G = 7.4 \times 10^{16}$ m^{-2}, and the twin thickness is $t = 1/\sqrt{\rho_G} = 3.7$ nm. The stabilization of the R phase at $d < 50$ nm and $\lambda < 50$ nm is related to the increase in the energy barrier of the *R–B*19' transformation (the second and third terms in Eq. (8)) that is caused by the sharp increase in the surface energy because of the generation of a high density of compound $\langle 100\rangle\{001\}$ twins, the increase in the stored elastic energy when martensite crystals inherit coherent disperse particles, and the particle-induced increase in the resistance to the motion of interphase boundaries. A decrease in the volume fraction of particles 20–40 nm in size increases interparticle distance λ, decreases the resistance to the motion of interphase boundaries during the MT, and decreases the density of geometrically necessary defects. At $d = 35 \pm 5$ nm and f = 4%, the density of compound $\langle 100\rangle\{001\}$ twins is $\rho_G = 2.6 \times 10^{16}$ m^{-2}. As a result, it follows from Eq. (8) that M_s increases as compared to the case of crystals with a high volume fraction of particles f (Fig. 5). In crystals with particles of size $d \ge 100$ nm, M_s increases as compared to the single-phase state and only weakly depends on the volume fraction of particles. Large disperse particles do not increase the resistance to the motion of interphase boundaries during the MT (see Table 2); the density of compound twins decreases as the particle size and interparticle distance increase (at $d = 400 \pm 20$ nm and f = 9%, $\rho_G = 0.7 \times 10^{16}$ m^{-2}); the critical martensite nucleus size (L_{nuc} = 15–50 nm [5, 24, 25]) becomes smaller than the interparticle distance λ; and the MT develops in the interparticle space. The same MT mechanism is observed in polycrystals with a grain size $D > 200$ nm [5]. Thus, in single crystals with particles of size d = 100–400 nm and λ = 100–400 nm and in polycrystals with a grain size $D > 200$ nm, the energy barrier of the *R–B*19' MT turns out to be significantly lower than that in crystals with a particle size d = 20–40 nm and λ = 20–50 nm and in polycrystals with a grain size $D < 100$ nm because of a decrease in the density of compound twins, a decrease in the elastic energy stored during the forward MT, and the presence of internal stresses (according to the fourth term in Eq. (8), they favor martensite nucleation on the particle–matrix interface). The temperature of the onset of the MT M_s in crystals with large particles (d = 100–400 nm) increases as compared to the single-phase state.

With Eqs. (3) and (4), we estimated $|\Delta G_{rev}|$ and $|\Delta G_{fr}|$ for heterophase Ti–Ni crystals (Fig. 7). We took into account that, when the MT develops in crystals with particles, the elastic and surface energies $|\Delta G_{rev}|$ are generated in a material during the nucleation of the first martensite plate at $T = M_s$ (the volume fraction of martensite is $\delta \longrightarrow 0$). In contrast to the single-phase single crystals, $|\Delta G_{rev}(0)| \ne 0$ [15]. Since disperse particles can serve as preferred nucleation sites for martensite crystals, martensite nucleates in the bulk of the material rather than on the free surface, and the appearance of the first martensite crystals is accompanied by the accumulation of the elastic and surface energies in the material. In crystals with large particles ($d \ge 100$–400 nm (f = 4–9%)), the reversible energy induced by the appearance of the first martensite crystals ($\delta \longrightarrow 0$) is $|\Delta G_{rev}(0)|$ = 5–15 J/mol and is independent of the volume fraction of particles (Fig. 7a). After the forward MT $\delta \longrightarrow 1$ $|\Delta G_{rev}(1)|$ increases more than sixfold as compared to $|\Delta G_{rev}(0)|$ and depends on the volume fraction of particles (Fig. 7b). At a low volume fraction of large particles ($f \le 5\%$), we have $|\Delta G_{rev}(1)|$ = 40–45 J/mol and $|\Delta G_{fr}|$ = 47–59 J/mol, which are close to the values found earlier for the single-phase crystals. Therefore, the development of the *R–B*19' MT in Ti–Ni crystals with large particles, where interparticle distance λ is larger than 400 nm, is qualitatively similar to that in the single-phase crystals. An increase in the volume fraction to f = 9% leads to an increase in both $|\Delta G_{rev}(1)|$ and $|\Delta G_{fr}|$ (see Fig. 7). In crystals with large particles of size $d > 100$ nm, the scattered energy exceeds the reversible energy accumulated during the development of the MT, $|\Delta G_{rev}(1)|/|\Delta G_{fr}|$ = 0.56–1.00, and the reverse MT occurs at $A_f > T_0$ due to chemical driving force $|\Delta G_{ch}|$.

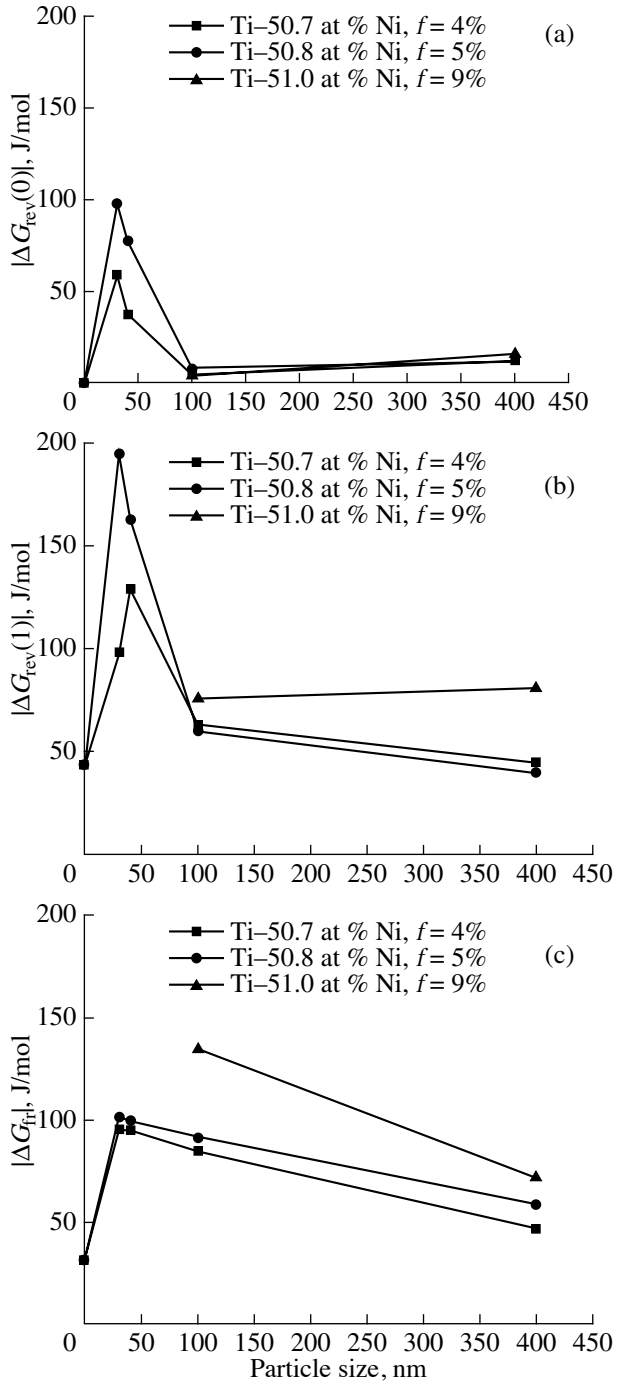

Fig. 7. Dependence of the nonchemical component of the free energy on the size and volume fraction of Ti_3Ni_4 particles during the development of the reversible MTs in aged Ti–(50.7–51.0) at % Ni single crystals: (a, b) reversible energy $|\Delta G_{rev}(0)|$ and $|\Delta G_{rev}(1)|$ for a volume fraction of martensite $\delta \longrightarrow$ (a) 0 and (b) 1, respectively, and (c) energy dissipation $|\Delta G_{fr}|$.

In crystals with small particles of size $d = 20$–40 nm and an interparticle distance $\lambda \leq 50$ nm (see Table 1), the development of the *R*–*B*19' MT is accompanied by a sharp (four- to eightfold) increase in $|\Delta G_{rev}(0)|$, $|\Delta G_{rev}(1)|$, and $|\Delta G_{fr}|$ as compared to the single-phase crystals (see Fig. 7). The ratio $|\Delta G_{rev}(1)|/|\Delta G_{fr}| = 1.4$–$1.8$ and the high level of stored energy $|\Delta G_{rev}(1)|$ favor the reverse *B*19'–*B*2 MT, which occurs at A_s and A_f below T_0.

The development of MTs in heterophase Ti–Ni crystals has a number of specific features that are not observed in the corresponding single-phase crystals. First, in the heterophase state, the temperature range of the forward MT Δ_1 exceeds the temperature range of the reverse MT Δ_2 ($\Delta_1 > \Delta_2$), and the temperature hysteresis depends on the volume fraction of martensite $\Gamma_2 = A_s - M_f(\delta \longrightarrow 1) > \Gamma_1 = A_f - M_s(\delta \longrightarrow 0)$. However, when the MTs develop in the single-phase crystals without an applied load, we have $\Delta_1 = \Delta_2$ and $\Gamma_1 = \Gamma_2$. The same hysteretic specific features are observed if the reversible MTs occur upon cooling/heating under applied stresses σ (Fig. 8) [26]. It is seen that, for single-phase crystals, $\Delta_1 = \Delta_2$ at $\sigma = 25$–160 MPa (Fig. 8a). In crystals with particles, the forward MT develops in two stages, which are related to the *B*2–*R* and *R*–*B*19' transformations, and the reverse *B*19'–*B*2 MT proceeds in one stage ($\Delta_1 > \Delta_2$). As a result, the strain–temperature curves are not parallel for the forward and reverse MTs (Fig. 8b), in contrast to quenched Ti–Ni crystals, where $\Delta_1 = \Delta_2$ and the slopes of the strain–temperature curves coincide (Fig. 8a). The low values of Δ_2 for the *B*19'–*B*2 MT without and with an applied load as compared to Δ_1 for the forward transition in heterophase crystals indicate differences in the development of the forward *R*–*B*19' and the reverse *B*19'–*B*2 MTs.

Figure 9 shows a schematic diagram for the MT development in Ti–Ni crystals with disperse particles. The MT develops in a matrix between disperse particles, and the matrix undergoes a uniform shear $\gamma = 0.130$ [3]. Since the particles do not undergo the MT and plastic deformation, the B19' martensite should be plastically deformed via compound $\langle 100 \rangle \{001\}$ twinning to retain the compatibility between the martensitic deformation of the matrix and the elastic deformation of the particles. This compound twinning should be considered as geometrically necessary defects in *B*19' martensite crystals. As a result, elastic and surface energies are generated in crystals with particles during the MT. For the reverse MT to develop, an energy barrier, which can be associated with the necessity of detwinning of *B*19' martensite crystals, must be overcome. Indeed, it was experimentally shown that the reverse MT requires a significant overheating; as a result, $\Gamma_2 = A_s - M_f$ exceeds $\Gamma_1 = A_f - M_s$. When the martensite undergoes detwinning, the elastic energy increases in the interparticle space, and this energy, in turn, favors an explosive kinetics of the reverse transformation. As a result, Δ_2 becomes smaller than Δ_1, and detwinning can be considered as the liberation of the elastic energy stored during the forward MT.

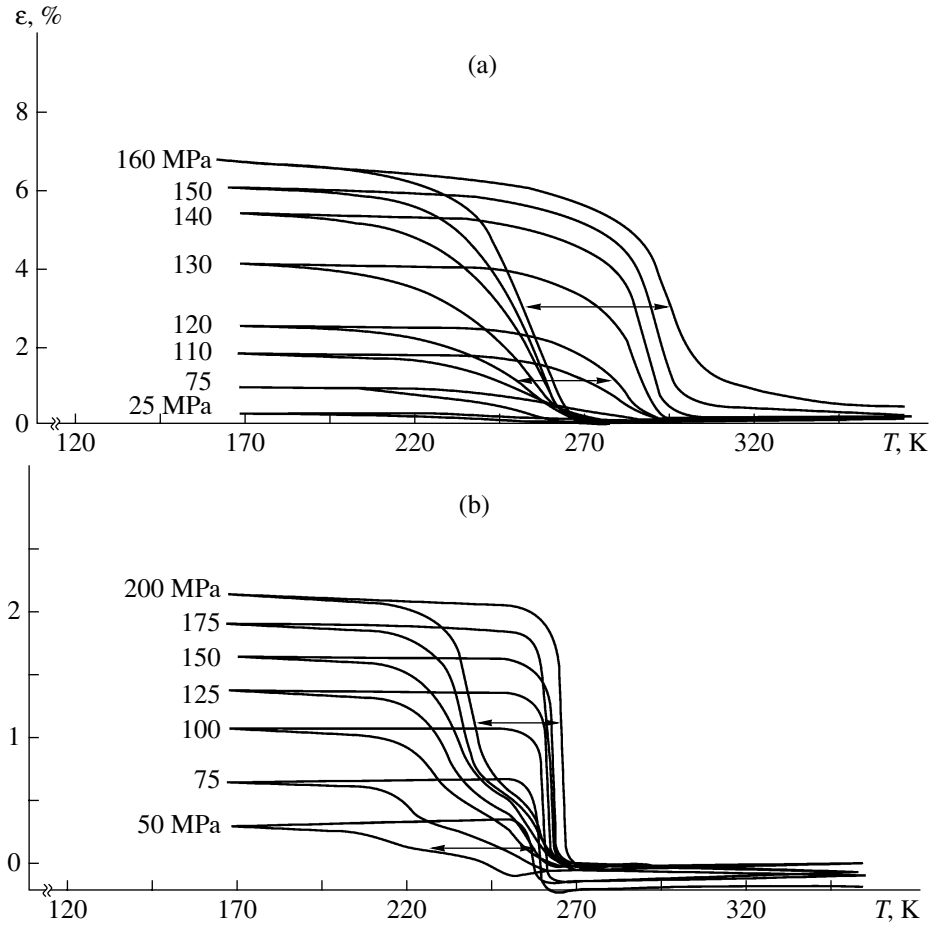

Fig. 8. Dependence of the temperature hysteresis on the applied constant load σ during the development of the *B*2–*B*19' and *B*2–*R*–*B*19' MTs: (a) in quenched Ti–50.1 at % Ni single crystals, orientation [$\bar{1}$11]; (b) in Ti–51.5 at % Ni single crystals aged at 823 K for 1.5 h, orientation [$\bar{1}$23].

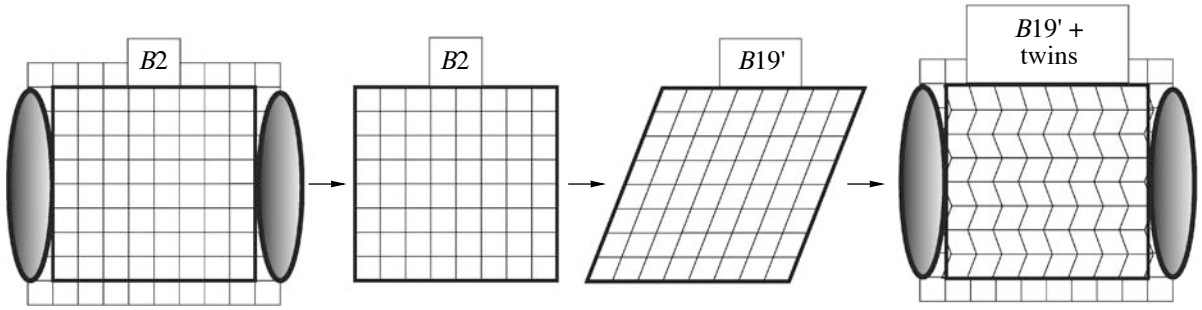

Fig. 9. Schematic diagram for the development of a thermoelastic MT in a heterophase crystal. Since Ti_3Ni_4 particles do not undergo the MT, the *R*–*B*19' transformation develops between the particles, and the interparticle region λ undergoes a uniform shear γ. We cut a cube with a side λ and subject it to shear deformation γ in a free-standing state. The cube (*B*2-phase single crystal) transforms into a parallelepiped (*B*19'-martensite single crystal). The parallelepiped cannot now be placed back into the cubic space from which it was cut. For the parallelepiped to be placed in the space and to be glued along its surface after the transformation, it must be deformed, for example, via the formation of geometrically necessary compound ⟨100⟩{001} twins.

Analogous specific features of the MT are observed in single-phase Ti–Ni polycrystals with a grain size D = 60–200 nm [5, 23]. In these nanomaterials, compound ⟨100⟩{001} twinning is the main type of twinning in the *B*19' martensite. As the grain size decreases (D < 50 nm), the *R*–*B*19' MT is fully suppressed, as in the case of crystals with particles of size λ ≤ 40–50 nm.

In crystals without disperse particles, polycrystals with a grain size $D > 200$ nm, and single crystals with large disperse particles ($d \geq 400$ nm, $\lambda \geq 360$ nm), the $B19'$ martensite contains no compound twins and has second-type $\langle 011 \rangle \{0.72053\ 1\ 1\}$ twins [6]. In these states, $\Delta_1 = \Delta_2$ and $\Gamma_1 = \Gamma_2$.

CONCLUSIONS

(1) In quenched single-phase Ti–(50.3–51.0) at % Ni single crystals, temperature M_s and chemical phase equilibrium temperature T_0 are determined by the nickel concentration in the crystals: as the Ni concentration decreases by 1 at %, they increase by 175 ± 10 K. When the $B2$–$B19'$ martensite transformations develop in quenched Ti–(50.3–51.0) at % Ni single crystals during cooling/heating in a free-standing state or at a constant applied load, the temperature ranges of the forward ($\Delta_1 = M_f - M_s$) and reverse ($\Delta_2 = A_f - A_s$) transformations and their temperature hystereses $\Gamma_1 = A_f - M_s$ and $\Gamma_2 = A_s - M_f$ coincide with each other, i.e., $\Gamma_1 = \Gamma_2$ and $\Delta_1 = \Delta_2$.

(2) In heterophase Ti–(50.7–51.0) at % Ni single crystals, the dependence of M_s on the size and volume fraction of Ti_3Ni_4 particles for the $R \longrightarrow B19'$ MTs is controlled by the following factors:

(a) a decrease in the nickel concentration in the matrix upon aging,

(b) the change in the resistance to the motion of interphase boundaries caused by disperse particles,

(c) the elastic and surface energies generated during the MTs,

(d) the internal stresses that appear because of the difference in the lattice parameters of the disperse particles and the matrix.

(3) In heterophase single crystals with Ti_3Ni_4 particles, the development of the forward R–$B19'$ martensite transformation in a free-standing state or at a constant applied load is characterized by a wider Δ_1 temperature range as compared to the temperature range of the reverse transformation Δ_2 ($\Delta_1 > \Delta_2$). Moreover, the temperature hysteresis $\Gamma_2 = A_s - M_f$ is larger than $\Gamma_1 = A_f - M_s$ ($\Gamma_2 > \Gamma_1$). The ratios Δ_1/Δ_2 and Γ_2/Γ_1 increase with the size and volume fraction of particles. At an interparticle distance $\lambda < 50$ nm, the R–$B19'$ MT is suppressed during cooling.

(4) We proposed a model to describe the dependence of the density of compound $\langle 100 \rangle \{001\}$ twins in $B19'$ martensite crystals on the interparticle distance λ and the grain size D. During the forward R–$B19'$ martensite transformation, compound twins appear to achieve the compatibility between the martensitic deformation of the matrix and the elastic deformation of the particles. For the reverse $B19'$–$B2$ transformation to begin, an energy barrier, which is associated with the detwinning of the martensite, must be overcome. This is possible at a significant overheating $\Gamma_2 = A_s - M_f$. The reverse transformation develops further according to an explosive kinetics with a small value of $\Delta_2 = A_f - A_s$ because of the liberation of the elastic energy during detwinning.

ACKNOWLEDGMENTS

We thank K. Otsuka and X. Ren for giving an opportunity to perform DSC measurements on their equipment.

This work was supported in part by the Russian Foundation for Basic Research, project no. 05-08-17915-a, 08-09-91952 NNIO-‡, and project no. DFG-MA 1175/25-1.

REFERENCES

1. *Shape Memory Materials*, Ed. by K. Otsuka and C. M. Wayman (Cambridge University Press, Cambridge, 1998).
2. V. G. Pushin, V. V. Kondrat'ev, and V. N. Khachin, *Pretransition Phenomena and Martensitic Transformations* (Ural. Otd. Ross. Akad. Nauk, Ekaterinburg, 1998) [in Russian].
3. K. Otsuka and X. Ren, "Physical Metallurgy of Ti–Ni-Based Shape Memory Alloys," Progr. Mater. Sci. **50**, 511–678 (2005)..
4. E. Hornbogen, V. Mertinger, and D. Wurzel, "Microstructure and Tensile Properties of Two Binary NiTi-Alloys," Scr. Mater. **44**, 171–178 (2001).
5. T. Waitz, T. Antretter, F. D. Fischer, et al., "Size Effects on the Martensitic Phase Transformation of NiTi Nanograins," J. Mech. Phys. Solids **55**, 419–444 (2007).
6. M. Nishida, C. M. Wayman, and A. Chiba, "Electron Microscopy Studies of Martensitic Transformation of an Aged Ti–51 at. % Ni Shape Memory Alloy," Metallography, No. 21, 275–291 (1988).
7. M. Nishida, C. M. Wayman, and T. Honma, "Precipitation Processes in Near-Equiatomic TiNi Shape Memory Alloys," Metall. Trans. A **17**, 1505–1515 (1986).
8. G. Fan, Y. Zhou, W. Chen, et al., "Precipitation Kinetics of Ti_3Ni_4 in Polycrystalline Ni-Rich Ti–Ni Alloys and Its Relation to Abnormal Multi-Stage Transformation Behavior," Mater. Sci. Eng., A **438–440**, 622–626 (2006).
9. G. Fan, W. Chen, S. Yang, et al., "Origin of Abnormal Multi-Stage Martensitic Transformation Behavior in Aged N-Rich Ti–Ni Shape Memory Alloys," Acta Mater. **52**, 4351–4362 (2004).
10. L. Bataillard, J.-E. Bidaux, and R. Gotthardt, "Interaction between Microstructure and Multiple-Step Transformation in Binary NiTi Alloys Using In-Situ Transmission Electron Microscopy Observations," Philos. Mag. A **78** (2), 327–344 (1998).
11. J. Michutta, Ch. Somsen, A. Yawny, et al., "Elementary Martensitic Transformation Processes in Ni-Rich NiTi Single Crystals with Ni_4Ti_3 Precipitates," Acta Mater. **54**, 3525–3542 (2006).
12. M. C. Carroll, Ch. Somsen, and G. Eggeler, "Multiple-Step Martensitic Transformations in Ni-Rich NiTi Shape Memory Alloys," Scr. Mater. **50**, 187–192 (2004).

13. A. Dlouhy, J. Khalil-Allafi, and G. Eggeler, "On the Determination of the Volume Fraction of Ti_3Ni_4 Precipitates in Binary Ni-Rich NiTi Shape Memory Alloys," Z. Metallkd. **95**, 518–524 (2004).
14. J. Khalil-Allafi, A. Dlouhy, and G. Eggeler, "Ni_4Ti_3-Precipitation during Aging of NiTi Shape Memory Alloys and Its Influence on Martensitic Phase Transformations," Acta Mater. **52**, 4351–4362 (2004).
15. J. Ortin and A. Planes, "Thermodynamic Analysis of Thermal Measurements in Thermoelastic Martensitic Transformations," Acta Mater. **36** (8), 1873–1889 (1988).
16. L. Daröczi, Z. Palänki, S. Szabö, and D. L. Beke, "Stress Dependence of Non-Chemical Free Energy Contributions in Cu–Al–Ni Shape Memory Alloy," Mater. Sci. Eng., A **378**, 274–277 (2004).
17. W. Tang, B. Sundman, R. Sandstrom, and C. Qiu, "New Modeling of the *B*2 Phase and Its Associated Martensitic Transformation in the Ti–Ni System," Acta Mater. **47** (12), 3457–3468 (1999).
18. E. Hornbogen, "The Effect of Variables on Martensitic Transformation Temperatures," Acta Mater. **33** (4), 595–601 (1985).
19. Yu. I. Chumlyakov, I. V. Kireeva, I. Karaman, et al., "Orientational Dependence of Shape Memory Effects and Superelasticity in CoNiGa, NiMnGa, CoNiAl, FeNiCoTi, and TiNi Single Crystals," Izv. Vyssh. Uchebn. Zaved., Fiz., No. 9, 4–20 (2004).
20. Yu. I. Chumlyakov, S. P. Efimenko, I. V. Kireeva, et al., "Effects of Shape Memory and Superelasticity in Aged TiNi Single Crystals," Dokl. Ross. Akad. Nauk **381** (5), 610–613 (2001) [Dokl. Phys. **46** (12), 849–852 (2001)].
21. V. V. Kokorin, *Magnetic Transformations in Inhomogeneous Solid Solutions* (Naukova Dumka, Kiev, 1987) [in Russian].
22. T. Waitz, "The Self-Accommodated Morphology of Martensite in Nanocrystalline NiTi Shape Memory Alloys," Acta Mater. **53**, 2273–2283 (2005).
23. A. F. Ashby, "The Deformation of Plastically Non-Homogeneous Materials," Philos. Mag. **21**, 399–424 (1970).
24. A. M. Glezer, E. N. Blinova, V. A. Pozdnyakov, and A. V. Shelyakov, "Martensite Transformation in Nanoparticles and Nanomaterials," J. Nanoparticle Res. **5**, 551–560 (2003).
25. K. Madangopal and J. Singh, "A Novel *B*19' Martensite in Nickel Titanium Shape Memory Alloys," Acta Mater. **48**, 1325–1344 (2000).
26. R. F. Hamilton, H. Sehitoglu, Y. H. J. Maier, and Y. I. Chumlykov, "Stress Dependence of the Hysteresis in Single Crystal NiTi Alloys," Acta Mater. **52**, 3383–3402 (2004).